PROCEEDINGS OF SPIE

SPIEDigitalLibrary.org/conference-proceedings-of-spie

Techniques to distinguish the ureter from the uterine artery in photoacoustic-guided hysterectomies

Alycen Wiacek, Karen C. Wang, Muyinatu A. Lediju Bell

Alycen Wiacek, Karen C. Wang, Muyinatu A. Lediju Bell, "Techniques to distinguish the ureter from the uterine artery in photoacoustic-guided hysterectomies," Proc. SPIE 10878, Photons Plus Ultrasound: Imaging and Sensing 2019, 108785K (27 February 2019); doi: 10.1117/12.2510716

SPIE.

Event: SPIE BiOS, 2019, San Francisco, California, United States

Techniques to distinguish the ureter from the uterine artery in photoacoustic-guided hysterectomies

Alycen Wiacek[a], Karen C. Wang[b], and Muyinatu A. Lediju Bell[a,c,d]

[a]Johns Hopkins University, Department of Electrical and Computer Engineering
[b]Johns Hopkins Medicine, Department of Gynecology and Obstetrics
[c]Johns Hopkins University, Department of Biomedical Engineering
[d]Johns Hopkins University, Department of Computer Science

ABSTRACT

Gynecologic surgery requires the clamping, cauterization, and transection of arteries that lie within millimeters of the ureter, posing significant potential risk for ureteral injury. By leveraging the optical absorption properties of hemoglobin and methylene blue (an FDA-approved contrast agent), we propose intraoperative photoacoustic imaging during hysterectomies to simultaneously visualize the uterine arteries and ureter, respectively. Three experiments were performed to test the feasibility of a spectroscopic system aimed at intraoperative visualization. At 690 nm, the contrast from blood and urine mixed with 200 uM methylene blue was 13.83 dB and 11.06 dB, respectively, representing a 2.77 dB contrast difference. Conversely, at 750 nm, the contrast from blood was similar (14.61 dB), and the contrast from urine mixed with 200 uM methylene blue decreased to 1.74 dB, which produced a greater contrast difference of 12.87 dB. When tissue was added, similar contrast differences were observed at these wavelengths. Finally, a laparoscopic tool was additionally visualized in real time in proximity to the ureter and uterine arteries, which supports the feasibility of a spectroscopic photoacoustic approach to differentiating the ureter from the uterine arteries in relationship to a laparoscopic tool during hysterectomies.

1. INTRODUCTION

Gynecologic surgery accounts for 75% of all intraoperative injuries to the ureters.[1] These injuries occur most often during the clamping, transection, or cauterization of the uterine arteries which are within millimeters of the ureter.[2] If these accidental injuries are noticed during the procedure, they can be addressed immediately to avoid serious complications and post operative sequelae. However, 50-70% of ureteral injuries are undetected during surgery, leading to additional surgeries, prolonged recovery, and even death. The most common practices to avoid injury to the ureter during a hysterectomy typically include mapping the anatomy by following the ureter through the pelvis, which is often followed by palpation in open surgery.[3,4] In laparoscopic surgery, avoiding ureteral injuries requires visualization of the ureter which may require entering the retroperitoneal space and ureterolysis.[5] More recently, groups have begun to use deep learning approaches to identify the ureter and the uterine artery in an endoscopic image.[6] While these techniques are beneficial for cases in which the anatomy is straightforward, they are time consuming and difficult when the anatomy is more challenging to discern, such as in patients with pelvic malignancies, cases with extensive adhesive disease from prior surgeries, or endometriosis. In in one retrospective study,[7] patients with pelvic malignancies, endometriosis, large ovarian masses, and pelvic inflammatory disease comprised 44% of ureter injuries, which suggests that these factors play a large role in ureter injury. In addition, greater than half of the patients with injuries to the ureter had no predisposing risk factors.

Photoacoustic imaging has shown promise with regard to identifying important structures during gynecological surgery.[8] In this technique, a target is illuminated using optical energy. Upon absorption of the optical energy, a mechanical pressure wave is generated and sensed by a standard ultrasound probe.[9] Due to the specific absorption properties of hemoglobin, photoacoustic imaging has proven successful in blood vessel detection.[10] Although previous work has demonstrated the feasibility of a photoacoustic approach to hysterectomies using the da Vinci surgical system,[8] techniques to simultaneously identify the ureter were never explored.

Due to the low optical absorption properties of urine,[11,12] the ureter is difficult to identify in photoacoustic images. One solution is to introduce an FDA-approved contrast agent – i.e., methylene blue – which has optical

Photons Plus Ultrasound: Imaging and Sensing 2019, edited by Alexander A. Oraevsky, Lihong V. Wang,
Proc. of SPIE Vol. 10878, 108785K · © 2019 SPIE · CCC code: 1605-7422/19/$18 · doi: 10.1117/12.2510716

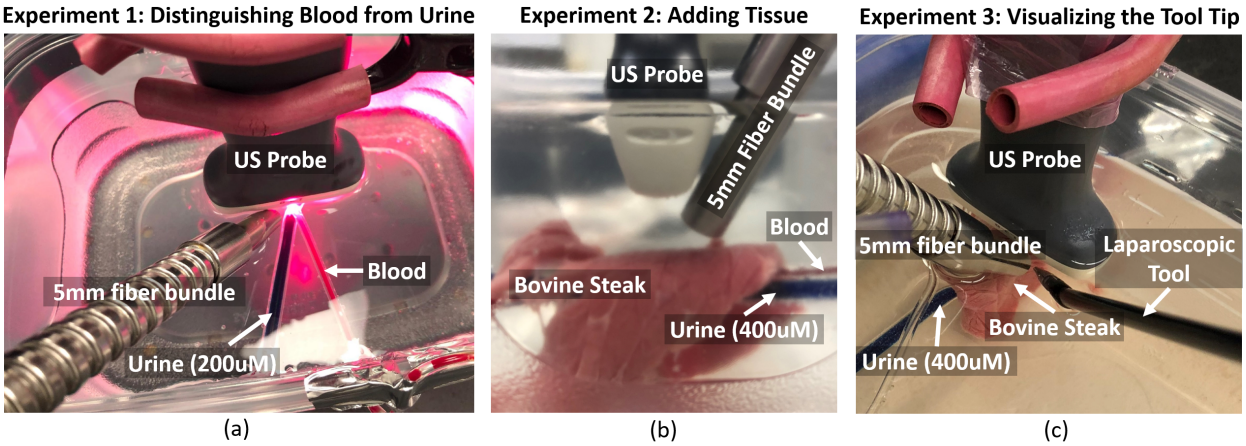

Figure 1: Experimental setup used for (a) Experiment 1, distinguishing blood from methylene blue in a water bath, (b) Experiment 2, continued visualization with added bovine steak tissue, and (c) Experiment 3, visualizing the laparoscopic tool tip in proximity to the mock ureter and uterine artery.

absorption peaks at 609 and 668 nm.[13] By leveraging the optical absorption properties of both hemoglobin and methylene blue, we propose photoacoustic imaging as a solution for intraoperative, simultaneous visualization of the ureter and the uterine artery during hysterectomies. This paper presents the results of three experiments aimed at characterizing the necessary system requirements to enable simultaneous visualization of the ureter and uterine artery.

2. METHODS

2.1 Experimental Setup

Three experiments were performed to assess the feasibility of distinguishing the ureter from the uterine artery: (1) distinguishing blood from urine in a water bath, (2) distinguishing blood from urine when both are surrounded by tissue, and (3) visualizing a laparoscopic grasper tool tip (Autosuture Endo Grasp, Medtronic, Fridley, MN) in addition to blood and urine surrounded by tissue.

Fig. 1 shows the experimental setup for each of the three experiments. In all three experiments a 1.59 mm inner diameter tube filled with *ex vivo* human blood was overlaid on a 3.96 mm inner diameter tube filled with urine and methylene blue (200 uM concentration for experiment 1 and 400 uM concentration for experiments 2 and 3). The inner diameter of each tube was selected to represent the diameters of the uterine artery[14] and the ureter,[15] respectively.

In each experiment, the photoacoustic imaging setup included an Alpinion ECUBE12R research ultrasound scanner, connected to an Alpinion L3-8 linear array ultrasound transducer with a transmit frequency of 8 MHz. A Phocus Mobile laser (Opotek, Inc., Carlsbad, CA) coupled to a 5 mm fiber bundle was used to illuminate the targets.

2.2 Data Acquisition and Analysis

Photoacoustic imaging was performed with wavelengths from 690 nm to 800 nm and energies that were lowered with each experiment (i.e., 40 mJ for Experiment 1, 25 mJ for Experiment 2, and 8 mJ for Experiment 3). Energies were lowered in the later experiments, because it was determined that lower energies produced sufficient contrast to visualize differences between the ureter and the uterine artery. Both ultrasound and photoacoustic channel data were saved for post processing.

Standard delay-and-sum (DAS) beamforming and short-lag spatial coherence (SLSC) beamforming were applied to create photoacoustic images. SLSC beamforming displays the spatial coherence of pressure waves[16] and has been shown to reduce clutter in both ultrasound and photoacoustic images.[17,18] SLSC beamforming is

performed after applying receive delays. The normalized cross-correlation between signals received by equally spaced elements (i.e., spatial lags) is then calculated with an axial kernel size, $k = n_2 - n_1$, that is equivalent to one wavelength.[19] Based on these details, the normalized spatial correlation is defined as:

$$\hat{R}(m) = \frac{1}{N-m} \sum_{i=1}^{N-m} \frac{\sum_{n=n_1}^{n_2} s_i(n) s_{i+m}(n)}{\sqrt{\sum_{n=n_1}^{n_2} s_i^2(n) \sum_{n=n_1}^{n_2} s_{i+m}^2(n)}} \tag{1}$$

where N is the number of elements in the transducer, m is the spatial lag in units of number of elements, $s_i(n)$ is a time-delayed, zero-mean signal received at element i from depth n. The resulting spatial coherence function is then summed up to a specific short-lag value, M, yielding the value of the SLSC image pixel. This process is repeated for each lateral and axial position in the image.

To assess the visibility of each signal, the wavelength was tuned from 690 to 800 nm, and contrast was measured as a function of wavelength as follows:

$$Contrast = 20 \log_{10} \left(\frac{S_i}{S_o} \right) \tag{2}$$

where S_i and S_o are the means of signals within regions of interest (ROIs) inside and outside of a target, respectively. The signal ROIs for this study were selected to be the same size as the inner tubing diameter. In addition, all ROIs were selected to avoid reflection artifacts or signals from the plastic tubing.

3. RESULTS

3.1 Distinguishing Blood from Urine

Fig. 2 shows the results from the first experiment, which aimed to differentiate blood from urine mixed with methylene blue in a controlled water bath experiment. Figs. 2(a) shows a photoacoustic image acquired with a wavelength of 690 nm overlaid on the ultrasound image. Similarly Fig. 2(c) shows a photoacoustic image acquired with a wavelength of 750 nm overlaid on the same ultrasound image. The wavelengths of 690 nm and 750 nm were chosen as example photoacoustic images based on the specific optical absorption peaks of methylene blue (668 nm) and hemoglobin (750 nm).

The ROIs defining the target signal for the contrast measurements is shown as the inner circles overlaid on each image. At a wavelength of 690 nm, the contrast from the blood and urine was 13.83 dB and 11.06 dB,

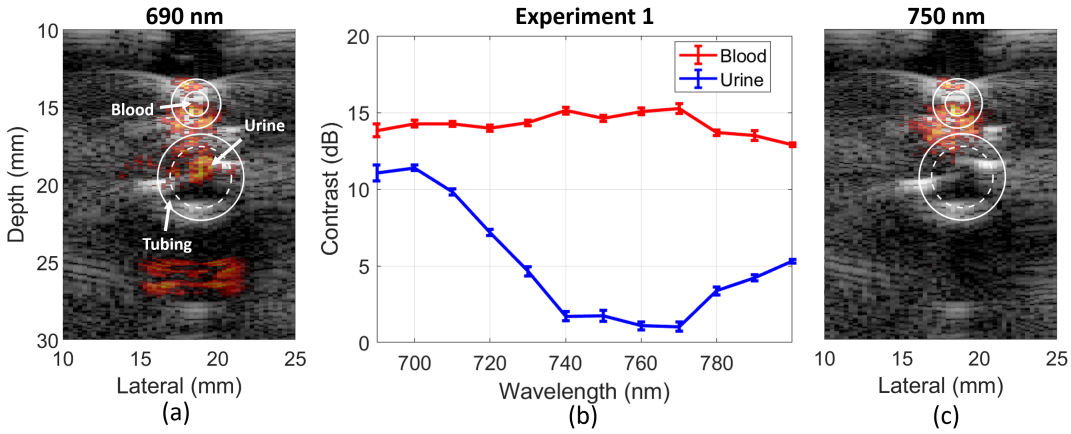

Figure 2: Experiment 1 results deomnstrating example photoacoustic images from overlapping tubes containing blood and urine mixed with methylene blue submerged in water at (a) 690 nm, (c) 750 nm wavelengths. The signal below the tubing in (a) is due to reflections from the methylene blue and the plastic tubing. (b) Contrast measurements as a function of wavelength.

respectively, resulting in a contrast difference of 2.77 dB. At a wavelength of 750 nm, the contrast from the blood and urine was 14.61 dB and 1.74 dB, respectively, resulting in a higher contrast difference of 12.87 dB, mostly due to the reduction in the contrast associated with the urine-filled tube. These quantitative metrics are confirmed with the corresponding images. In particular, at a wavelength of 690 nm (i.e., Fig. 2(a)), the photoacoustic signal is largely present in the center of the bottom tube containing methylene blue and urine. However, at a wavelength of 750 nm (i.e., Fig. 2(c)), there is no signal present in the bottom tube (although signal remains in the top tube containing blood). The presence of the urine signal at 690 nm and not at 750 nm supports a spectroscopic approach that dynamically switches between 690 nm and 750 nm in order to differentiate between the ureter and the uterine artery.

The same ROIs described above were used to calculate contrast for all wavelengths. Fig. 2(b) shows the measured contrast as a function of wavelength from 690 nm to 800 nm. The contrast of the blood signal is consistently greater than that of the urine signal at these wavelengths, particularly at 750 nm.

3.2 Adding Tissue

Fig. 3 shows the results from the second experiment, in which bovine steak was added to the set up from the first experiment with the goal of assessing blood and urine differentiation in the presence of tissue. In particular, Figs. 3(a) and 3(c) show photoacoustic images acquired with 690 nm and 750 nm wavelengths, respectively, each overlaid on the same ultrasound image. Similar to Experiment 1, at 690 nm, the average contrast difference between blood and urine mixed with methylene blue was 4.4 dB. At 750 nm, the average contrast difference between blood and urine mixed with methylene blue was 21.2 dB. The photoacoustic images are consistent with these quantitative measurements, displaying signals inside of the bottom tube at 690 nm (i.e., Fig. 3(a)), which are largely absent at 750 nm (i.e., Fig. 3(c)).

When adding tissue, the reflections from the tubing that were present in Fig. 2(a) are minimized. However, it is more difficult to localize the signal due to the additional sidelobes. To mitigate these artifacts, SLSC beamforming was applied, as shown in Figs. 3(d)-3(f). The mean contrast differences between blood and urine

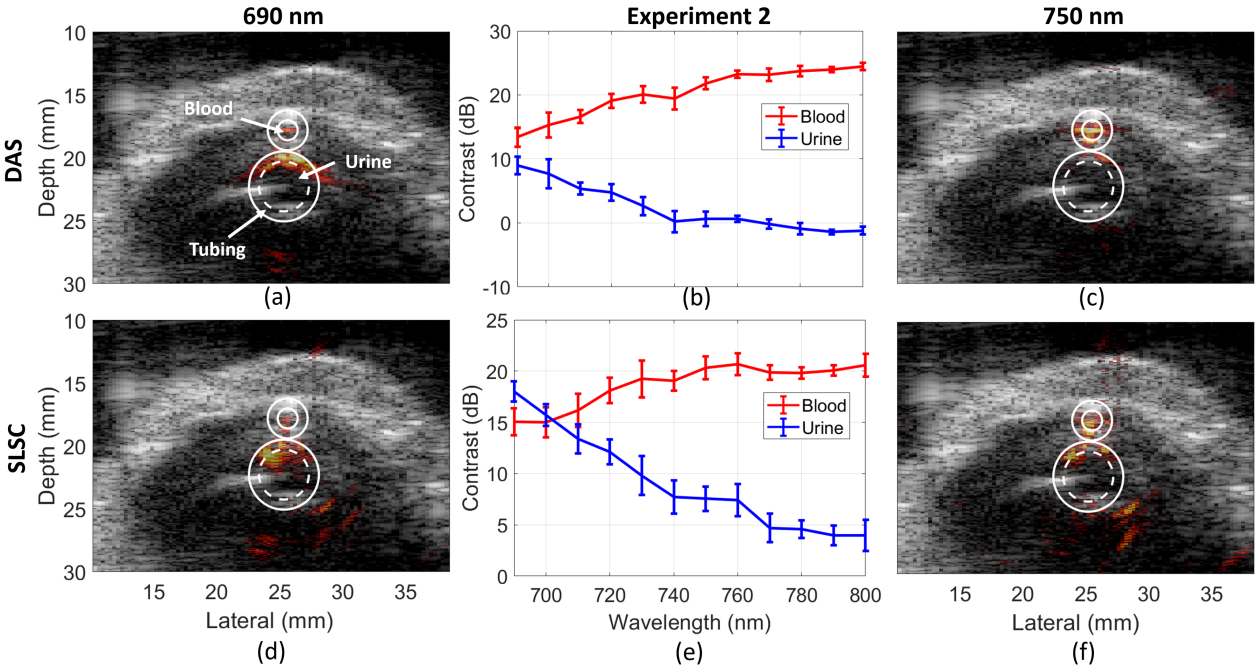

Figure 3: Experiment 2 results demonstrating example photoacoustic images and the associated contrast mesaurements obtained using (a-c) delay-and-sum (DAS) beamforming and (d-f) short-lag spatial coherence (SLSC) beamforming ($M = 20$).

mixed with methylene blue are 1.3 dB and 14.1 dB at 690 nm and 750 nm wavelengths, respectively. This difference is consistent with the presence of the urine and methylene blue signal in images acquired with a wavelength of 690 nm (Fig. 3(d)) and the absence of this signal in images acquired with a wavelength of 750 nm (Fig. 3(f)). The contrast measured at multiple wavelengths for images created with DAS and SLSC beamforming is shown in Figs. 3(b) and 3(e), respectively. Similar to the first experiment, the contrast of the blood signal is greater than that of the urine mixed with methylene blue signal for a majority of the wavelengths.

Fig. 4 shows the contrast of both blood and urine mixed with methylene blue, as a function of the laser wavelength for multiple tissue thicknesses. When imaging in the presence of 2 mm-thick tissue, there is a 21.16 dB contrast difference between the signals associated with urine and blood at 750 nm wavelength (see Fig. 4(a)). When an additional 2 mm of tissue is added (4 mm total), the of the blood signal significantly decreases and the contrast difference between the signals associated with blood and urine significantly decreases to 3.47 dB at 750 nm wavelength, as shown in Fig. 4(b). Finally with 6 mm of tissue, the contrast values overlap (see Fig. 4(c)), indicating an inability to differentiate the two signals.

3.3 Including the Laparoscopic Tool

Fig. 5 shows the results from the third experiment in which the laparoscopic tool was introduced. Figs. 5(a) and 5(c) show SLSC photoacoustic images acquired with 690 nm and 750 nm wavelengths, respectively, overlaid

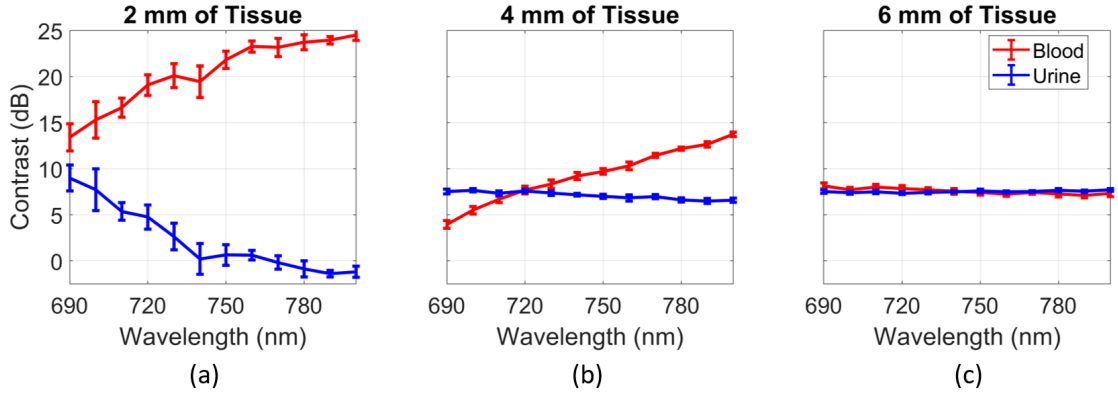

Figure 4: Contrast as a function of wavelength in the presence of (a) 2mm, (b) 4mm, and (c) 6mm tissue thickness. Measurements were obtained using DAS beamforming.

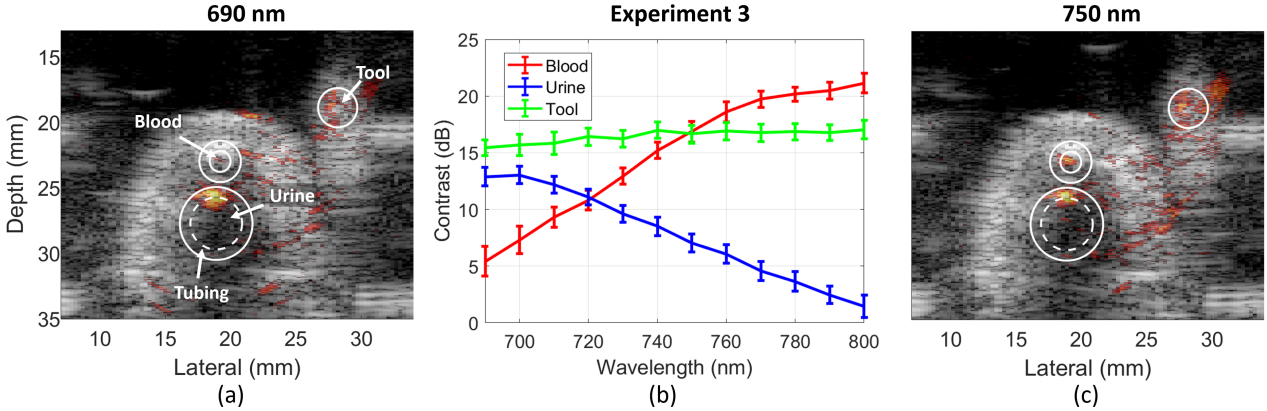

Figure 5: Experiment 3 results demonstrating example photoacoustic images acquired with (a) 690 nm, (c) 750 nm laser wavelengths. The signals on the right side of both (a) and (c) are due to reflections from the tubing and the speed of sound differences at the water-tissue boundaries. (b) Contrast measurements as a function of wavelength using SLSC beamforming ($M = 20$).

on the same ultrasound image. Fig. 5(b) shows the measured contrast as a function of wavelength for the blood, urine, and the laparoscopic tool using the ROIs shown in Figs. 5(a) and 5(c).

At 690 nm, the average contrast of the tool, urine, and blood were, 15.44 dB, 12.89 dB, and 5.42 dB, respectively. At 750 nm, the average contrast of the tool, urine, and blood were, 16.66 dB, 7.06 dB, and 16.85 dB, respectively. The photoacoustic signals to the right of the laparoscopic tool are due the illumination of the metal tool tip located outside of the ultrasound imaging plane, resulting in out-of-plane photoacoustic signals being received by the transducer. Despite these signals, the contrast of the metal tool located within the indicated ROI remains relatively constant across wavelengths as demonstrated in Fig. 5(b). In addition, as demonstrated in the previous two experiments, the contrast difference between the blood and methylene blue are distinguishable when comparing the 690 nm result (7.48 dB contrast difference) to the 750 nm result (9.79 dB contrast difference), despite the contrast of the blood signal being lower than that in the first two experiments due to the lower laser energy.

4. DISCUSSION

The measured contrast differences between urine mixed with methylene blue and blood at 690 and 750 nm wavelengths demonstrate that photoacoustic imaging is a promising technique to distinguish between the ureter and the uterine artery. In particular, this differentiation would be best achieved by dynamically switching between these two wavelengths during the procedure. A quantitative spectroscopic approach such as this would allow the ureter to be identified at 690 nm and then immediately differentiated from the uterine artery when switching to 750 nm due to the large signal change (i.e., >14 dB decrease in contrast, as shown in Fig. 3).

When these targets are surrounded by tissue, the differentiation between true signal and noise can be challenging due to reflection artifacts from the tubing as well as absorption from the surrounding tissue. The incoherent noise sources present can be mitigated by applying SLSC beamforming, which further enhances the true signal and suppresses noise. As tissue thickness increases, the true signals are more difficult to differentiate. As a result, this system can identify and distinguish the ureter from the uterine artery with <4mm of tissue present, which is typical in hysterectomy procedures.

One limitation of the presented experiments is the presence of photoacoustic signals from the plastic tubing. Although the effect of this signal was mitigated by using ROIs of the same size as the inner diameter of the tube, the resulting image is more difficult to interpret with the signal from the tubing present. Future *in vivo* studies will help to reduce this confusion by removing the need for plastic tubing.

In addition to our success with quantitative differentiation of urine and blood, both the tool tip and the urine were identifiable in photoacoustic images. The tool tip can additionally be identified with real-time photoacoustic imaging as the surgeon moves the tool. The distance between the identified tool tip and the ureter can then be measured. It is of particular importance to surgeons to know when the tool tip is in close proximity to the ureter, which places the ureter at a higher risk of injury. Therefore, our future work will explore auditory feedback as the tool approaches the ureter. Providing this auditory information to the surgeon will diminish the requirement to visualize the additional information provided by the proposed photoacoustic approach.

5. CONCLUSION

This work is the first to investigate photoacoustic imaging as a viable option to assist with the distinction of the ureter and uterine artery during hysterectomies. The optical absorption properties of hemoglobin and methylene blue are the key enabling factors of the proposed approach to use photoacoustic imaging to reduce the risk of ureteral injury during hysterectomies. Results demonstrate the feasibility of photoacoustic-based methods to distinguish the ureter (when methylene blue is introduced into the urinary tract), uterine artery, and the laparoscopic tool in the presence of <4mm of tissue thickness.

Acknowledgements

This work is supported by a Johns Hopkins Discovery Award.

REFERENCES

[1] Dowling, R. A., Corriere Jr, J. N., and Sandler, C. M., "Iatrogenic ureteral injury," *The Journal of Urology* **135**(5), 912–915 (1986).

[2] Williams, P. L., Bannister, L., Berry, M., Collins, P., Dyson, M., Dussek, J., and Ferguson, M., "Grays anatomy: the anatomical basis of medicine and surgery," *Edinburgh: Churchill Livingstone* **38**, 1560 (1995).

[3] Chan, J. K., Morrow, J., and Manetta, A., "Prevention of ureteral injuries in gynecologic surgery," *American Journal of Obstetrics and Gynecology* **188**(5), 1273–1277 (2003).

[4] Manetta, A., "Surgical maneuver for the prevention of ureteral injuries," *Journal of Gynecologic Surgery* **5**(3), 291–294 (1989).

[5] Jelovsek, J. E., Chiung, C., Chen, G., Roberts, S. L., Paraiso, M. F. R., and Falcone, T., "Incidence of lower urinary tract injury at the time of total laparoscopic hysterectomy," *JSLS: Journal of the Society of Laparoendoscopic Surgeons* **11**(4), 422 (2007).

[6] Harangi, B., Hajdu, A., Lampe, R., and Torok, P., "Differentiating ureter and arteries in the pelvic via endoscope using deep neural network," in [*10th International Symposium on Image and Signal Processing and Analysis (ISPA), 2017*], 86–89, IEEE (2017).

[7] Liapis, A., Bakas, P., Giannopoulos, V., and Creatsas, G., "Ureteral injuries during gynecological surgery," *International Urogynecology Journal* **12**(6), 391–394 (2001).

[8] Allard, M., Shubert, J., and Bell, M. A. L., "Feasibility of photoacoustic-guided teleoperated hysterectomies," *Journal of Medical Imaging* **5**(2), 021213 (2018).

[9] Beard, P., "Biomedical photoacoustic imaging," *Interface Focus* **1**(4), 602 (2011).

[10] Hoelen, C., De Mul, F., Pongers, R., and Dekker, A., "Three-dimensional photoacoustic imaging of blood vessels in tissue," *Optics Letters* **23**(8), 648–650 (1998).

[11] Feng, S., Chen, W., Li, Y., Chen, G., Huang, Z., Liao, X., Xie, Z., and Chen, R., "Surface-enhanced raman spectroscopy of urine by an ingenious near-infrared raman spectrometer," in [*Optics in Health Care and Biomedical Optics III*], **6826**, 682628, International Society for Optics and Photonics (2008).

[12] Huang, M.-C., Sun, H.-W., et al., "Study of normal and cancerous urine using photoacoustic spectroscopy," *Journal of Biomedical Engineering* **12**(5), 425–428 (1990).

[13] Matsui, A., Tanaka, E., Choi, H. S., Kianzad, V., Gioux, S., Lomnes, S. J., and Frangioni, J. V., "Real-time, near-infrared, fluorescence-guided identification of the ureters using methylene blue," *Surgery* **148**(1), 78–86 (2010).

[14] Obimbo, M. M., Ogengo, J. A., and Saidi, H., "Comparative regional morphometric changes in human uterine artery before and during pregnancy," *Pan African Medical Journal* **13**(1) (2012).

[15] Zelenko, N., Coll, D., Rosenfeld, A. T., and Smith, R. C., "Normal ureter size on unenhanced helical ct," *American Journal of Roentgenology* **182**(4), 1039–1041 (2004).

[16] Lediju, M. A., Trahey, G. E., Byram, B. C., and Dahl, J. J., "Short-lag spatial coherence of backscattered echoes: Imaging characteristics," *IEEE Transactions on Ultrasonics, Ferroelectrics, and Frequency Control* **58**(7) (2011).

[17] Bell, M. A. L., Kuo, N., Song, D. Y., and Boctor, E. M., "Short-lag spatial coherence beamforming of photoacoustic images for enhanced visualization of prostate brachytherapy seeds," *Biomedical optics express* **4**(10), 1964–1977 (2013).

[18] Pourebrahimi, B., Yoon, S., Dopsa, D., and Kolios, M. C., "Improving the quality of photoacoustic images using the short-lag spatial coherence imaging technique," in [*Photons Plus Ultrasound: Imaging and Sensing 2013*], **8581**, 85813Y, International Society for Optics and Photonics (2013).

[19] Bell, M. A. L., Dahl, J. J., and Trahey, G. E., "Resolution and brightness characteristics of short-lag spatial coherence (slsc) images," *IEEE Transactions on Ultrasonics, Ferroelectrics, and Frequency Control* **62**(7), 1265–1276 (2015).